Maneuvering Mineralization of Self-assembled Peptide Nanofibers for Designing Mechanically-stiffened Self-healable Composites toward Bone-mimetic ECM

Nimisha A. Mavlankar,[a] Debasish Nath,[a] Yadu Chandran,[b] Nidhi Gupta,[a] Ashmeet Singh,[a] Viswanath Balakrishnan[b] and Asish Pal*[,a]

[a] Chemical Biology Unit, Institute of Nano Science and Technology, Knowledge City, Sector 81, Mohali, Punjab-140306, India

[b] School of Mechanical and Material Engineering, Indian Institute of Technology-Mandi, Kamand, Himachal Pradesh, India

*Corresponding author. E-mail: apal@inst.ac.in

Table of Contents

1. **Materials and methods** 2
2. **Synthesis and Characterization by HPLC-MS** 2
3. **Self-Assembly Kinetics through CD** 4
4. **Comparative estimation of % β-sheet** 5
5. **Fluorescence spectra with Thioflavin T** 6
6. **AFM Height profile for C_8PA** 6
7. **FT-IR for reactants in bioglass formation** 7
8. **XRD for C_nPA** 8
9. **Raman Spectra for C_nPA** 8
10. **XPS for C_nBG** 9
11. **EDX for C_nBG** 10
12. **Rheological studies** 11
13. **Plasticity index from Nanoindentation** 14
14. **Bioactivity study: TEM elemental Mapping** 15
15. **Bioactivity study: SEM** 16
16. **Bioactivity study: XRD** 17
17. **Bioactivity study: FT-IR** 18
18. **Bioactivity study: EDX** 19
19. **Cell culture studies: Optical Images** 20
20. **Cell culture studies: FDA/PI stained fluorescence images** 21
21. **Mineralization studies: ARS Staining** 22

Materials & Methods:

All Fmoc protected amino acids, activator (diisopropyl carbodiimide), piperazine, hexanoic acid, octanoic acid, decanoic acid, dodecanoic acid, triisopropylsilane, 1,2-ethanedithiol, tetraethyl orthosilicate (TEOS), triethyl phosphate (TEP), 4-dimethylaminopyridine (DMAP), *N,N*'-diisopropylcarbodiimide (DIC) and Hanks balanced salt solution were purchased from Sigma Aldrich. Oxyma, Fmoc-Rink amide MBHA resin, water, ethanol and DMF, were obtained from Merck. Trifluoroacetic acid (TFA) was purchased from SRL chemicals. Hexafluoroisopropanol (HFIP) was purchased from TCI chemicals. Anhydrous sodium sulphate and calcium sulphate were procured from Emparta and SD Fine chemicals ltd. respectively.

Synthesis and Characterization of the Peptide: Peptide amphiphiles **C_6PA, C_8PA, C_{10}PA, C_{12}PA** were synthesized using Microwave Automated Solid Phase Peptide Synthesizer (Liberty Blue CEM, Matthews, NC, USA). Fmoc-Rink Amide MBHA Resin was swelled in DMF for 30 minutes. All Fmoc protected amino acids were weighed as per for 0.1 mM scale of the reaction followed by dissolving in required DMF solution. Required mass of piperazine was vortexed in 10% of ethanol followed by addition of the remaining 90% of DMF for completely solubilization. DIC (activator) and oxyma (activator base) in DMF, were used for the coupling reaction between acid and amine to form the peptide bond. Deprotection of Fmoc group from the amino acid was achieved by using 20% piperazine in DMF containing 10% ethanol in the microwave reactor. A cycle of coupling, deprotection steps was repeated to synthesize the required peptide anchored to the resin. The aliphatic fatty acid spacers were coupled by deprotecting the *N*-terminal Fmoc followed by sequential double coupling with suitable activated acids (hexanoic acid/octanoic acid/decanoic acid/dodecanoic acid) with no final deprotection step. The peptide was then cleaved from the resin upon a slow shaking in a cocktail solution, a mixture of TFA/TIPS/water (95: 2.5: 2.5, %v/v/v) for 3 h at room temperature. The resin was then filtered and the filtrate was collected, containing desired peptide in the cocktail solution. The excess TFA was evaporated using air blower. The peptides **C_6PA**, **C_8PA**, **C_{10}PA**, **C_{12}PA** were then precipitated from cold diethyl ether and precipitate were washed using cold diethyl ether thrice. These were kept overnight to obtain white dried powder of the peptides. The peptides were purified by RP-HPLC using a Waters semi-preparative binary HPLC system using a Nucleodur C18-reverse phase column with an acetonitrile-water mobile phase containing 0.1% TFA. ESI/MS was performed with Waters Acquity QDa detector. Pure dried peptides were then dissolved in HFIP and was evaporated to erase self-assembly history of the peptides during purification/ freeze drying process.

Characterization by HPLC-MS

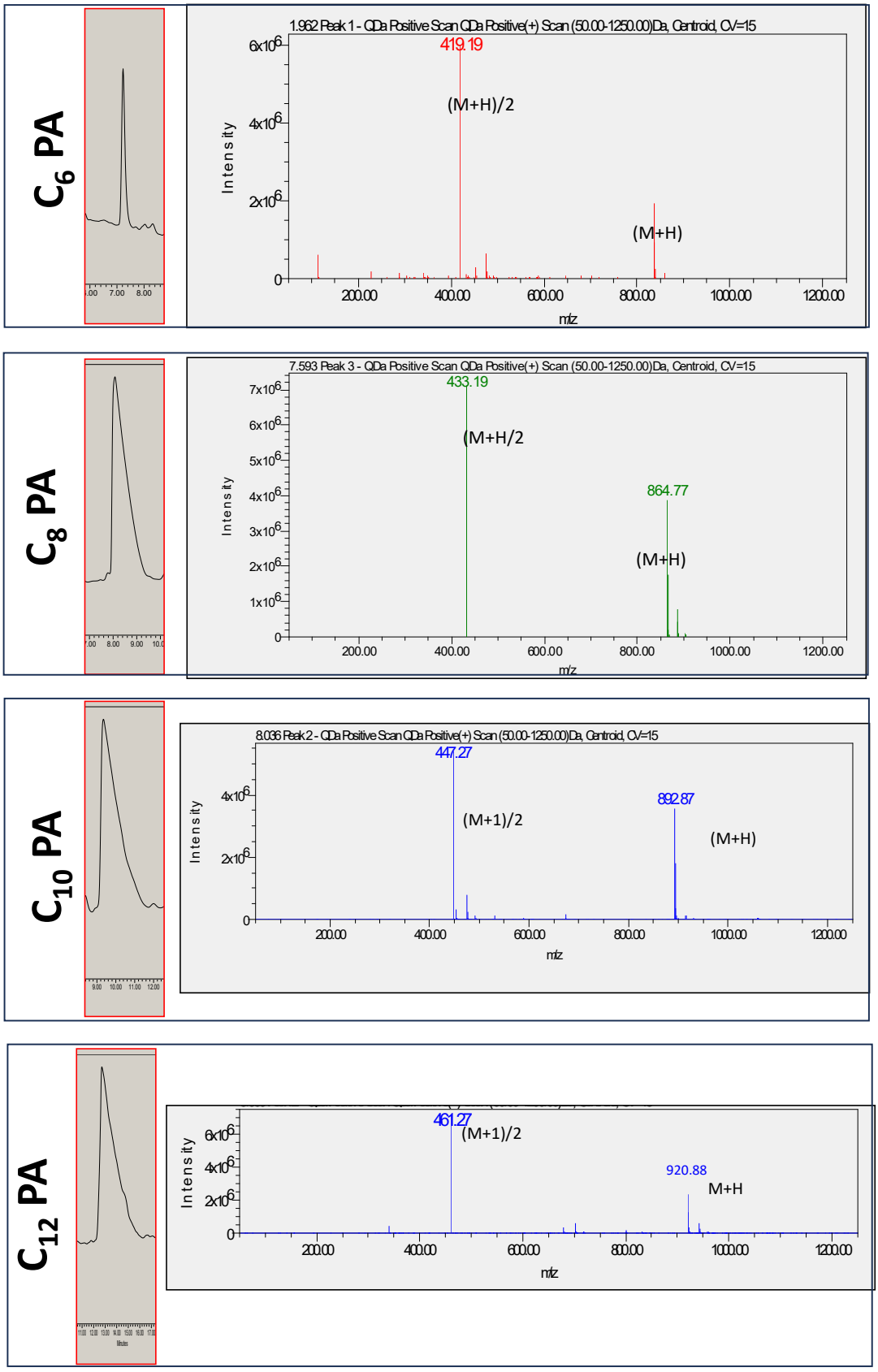

Figure S1: HPLC-Mass traces for **C_nPAs**.

Time dependent CD Studies

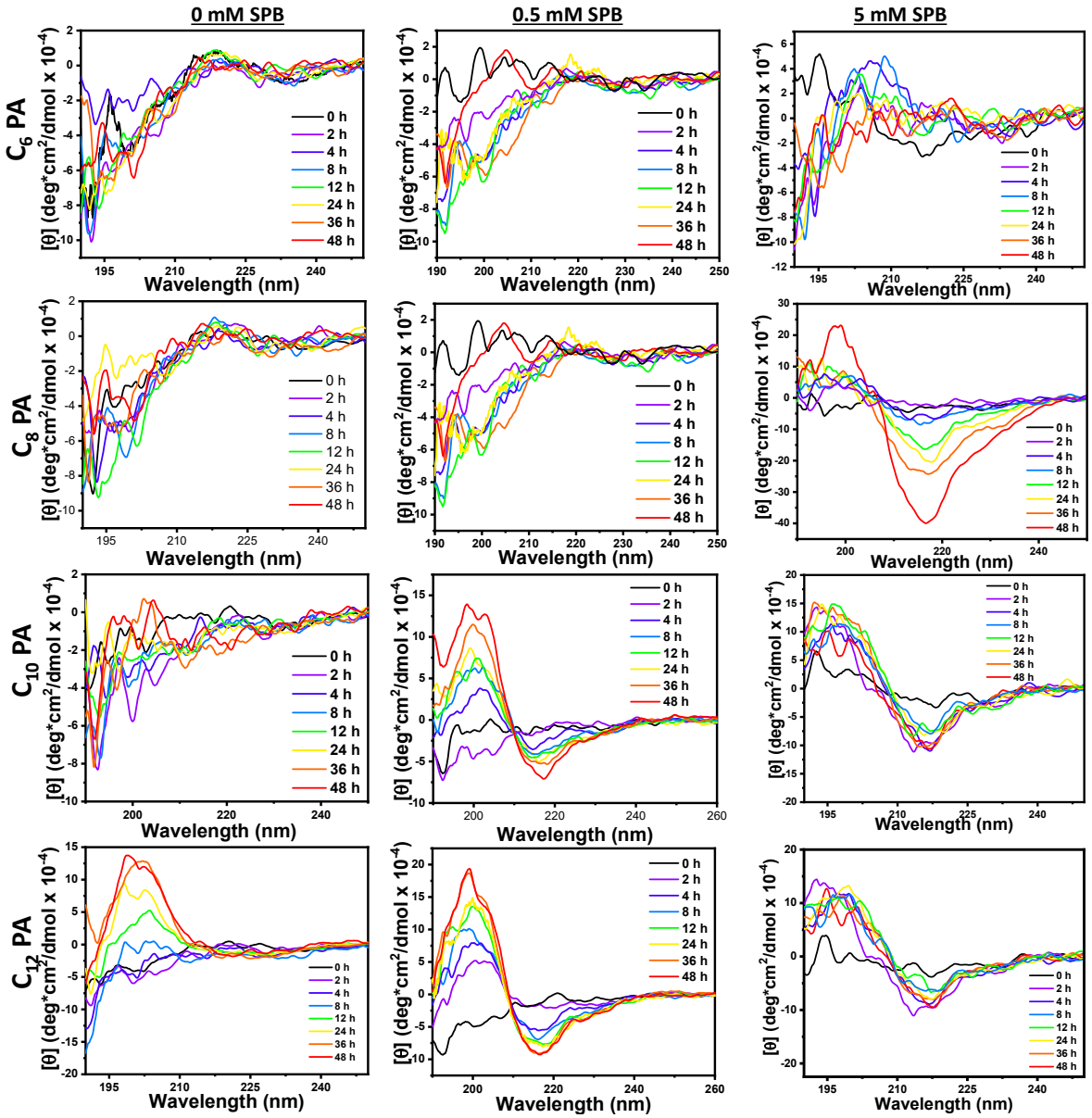

Figure S2: Kinetics of self-assembly monitored through CD spectra over 48 h for **C_6PA, C_8PA, C_{10}PA** and **C_{12} PA** at different ionic strengths of Sodium Phosphate Buffer. (c = 0.05 mM, T = 25 °C)

Secondary structure estimation

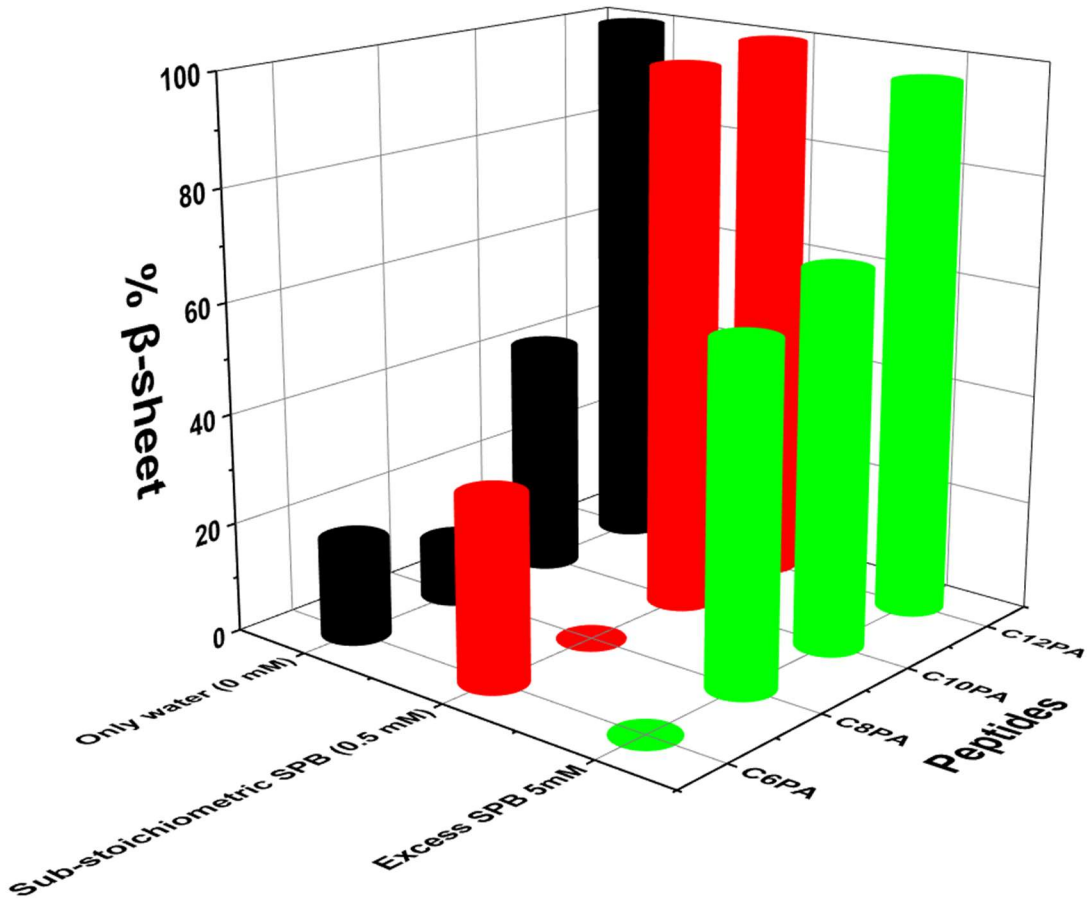

Figure S3: % β-sheet as dictated by the hydrophobicity and ionic strength for **C_nPA**. *(c* = 0.05 mM, T = 25 °C*)* Data represented are calculated from the spectra averaged from three acquisitions.

Fibrillization kinetics from Thioflavin T

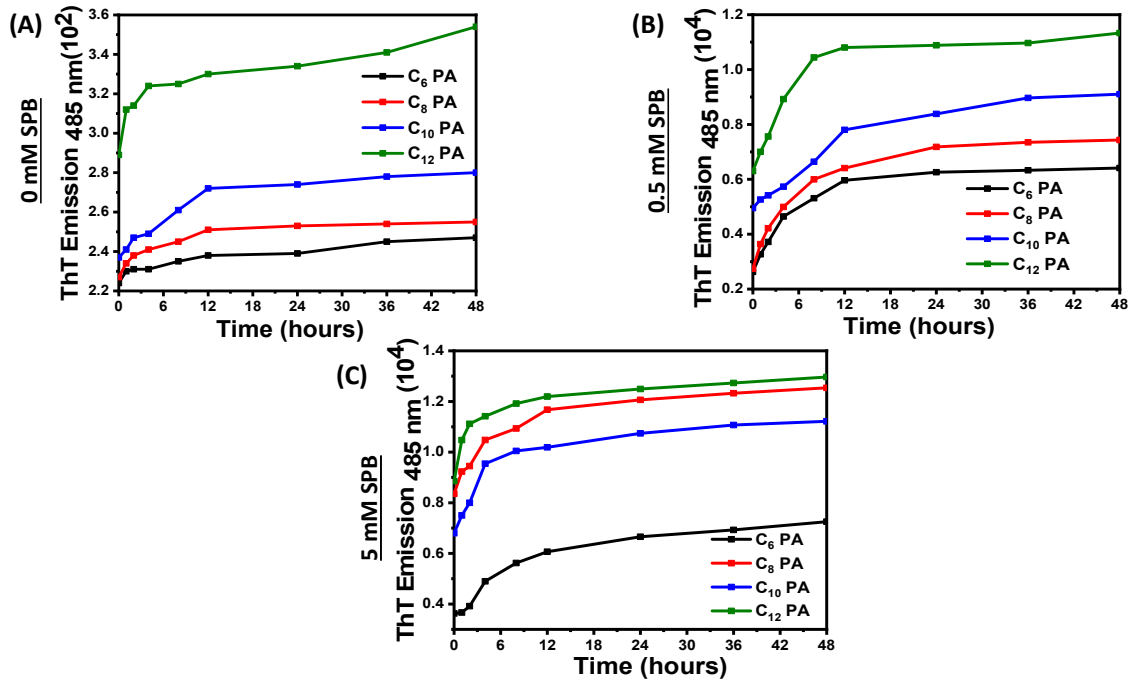

Figure S4: Thioflavin-T fluorescence spectra for **C_nPA** depicting amyloid growth over time (A) in water and in presence of (B) substoichimetric (0.5 mM) (C) excess amount of SPB. [**C_nPA**] = 0.5 mM and [ThT] = 0.025 mM (λ_{Ex} = 440 nm and λ_{Em} = 485 nm). Data represented are mean from triplicate samples.

AFM height profile

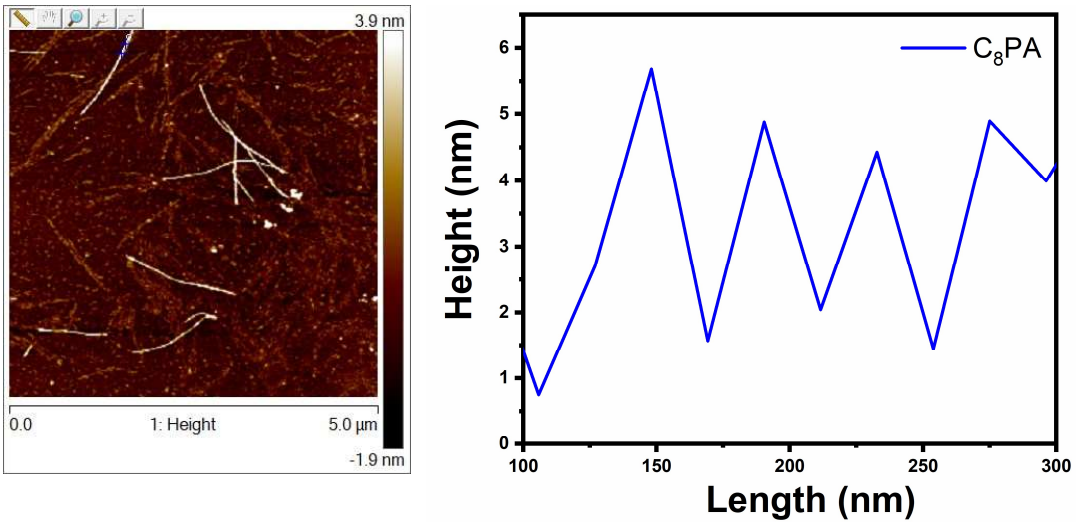

Figure S5: Height profile showing up-down trajectory of the twisted bundle morphology for **C_8PA** wherein twisting depicts a tightly packed, highly ordered structure. Height profile is reproducibly calculated from 25 different fibers imaged in three different areas.

FTIR controls of reactants used in the biomineralization process

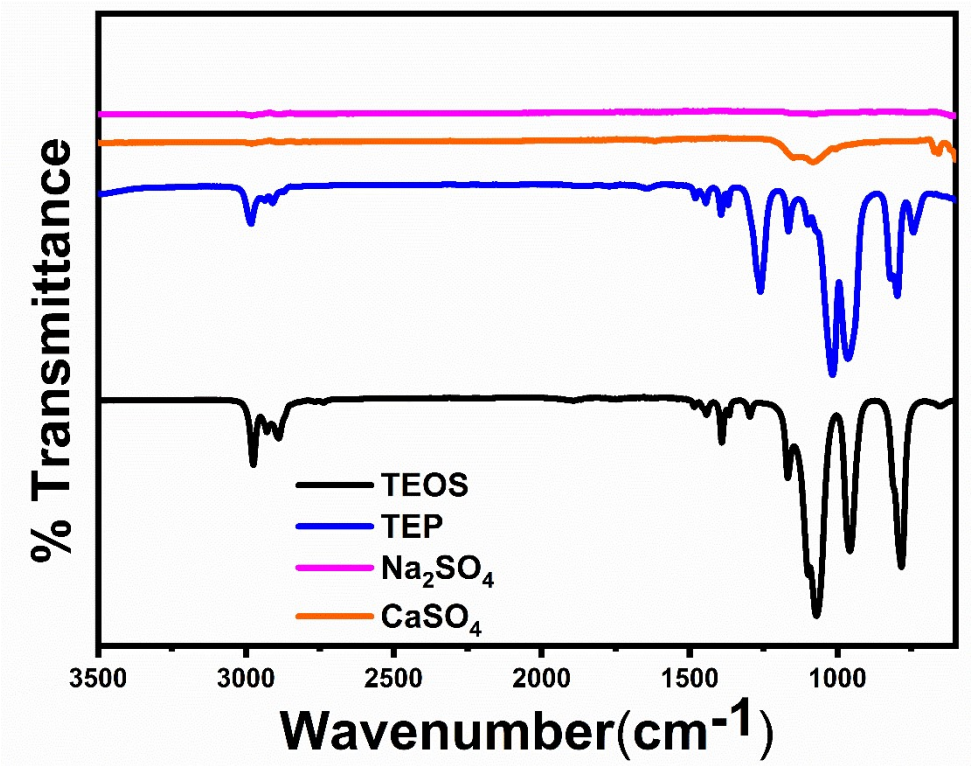

Figure S6: FT-IR spectra of bioglass precursors *viz.* TEOS (Tetraethyl orthosilicate) and TEP (Triethyl phosphate) as the glass network former, sodium and calcium sulphate as the glass network modifiers.

Structural elucidation of peptides before biomineralization

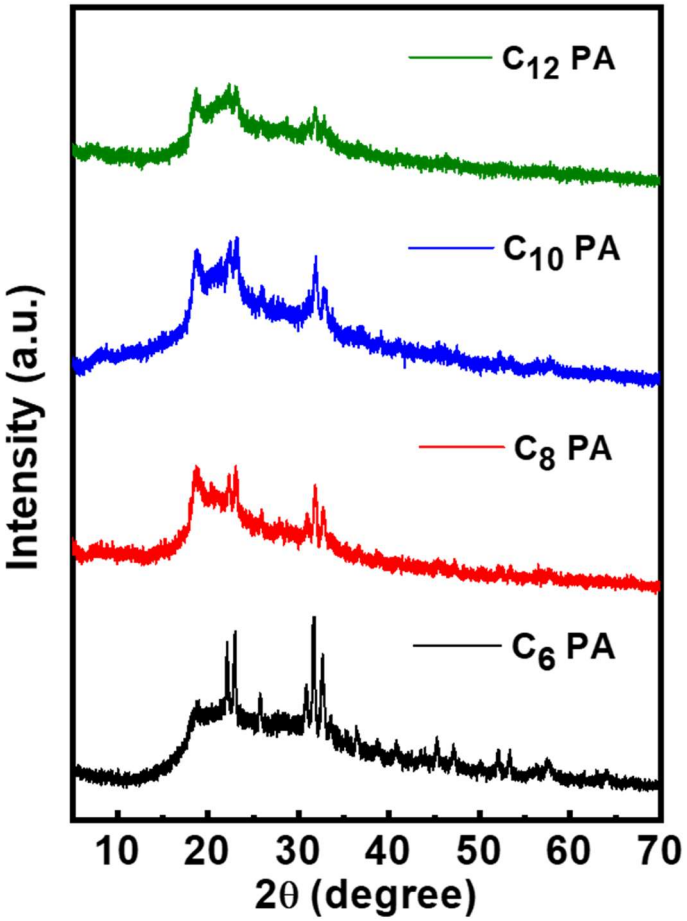

Figure S7: XRD spectra showing amorphous nature of peptide amphiphiles, **C_nPA**.

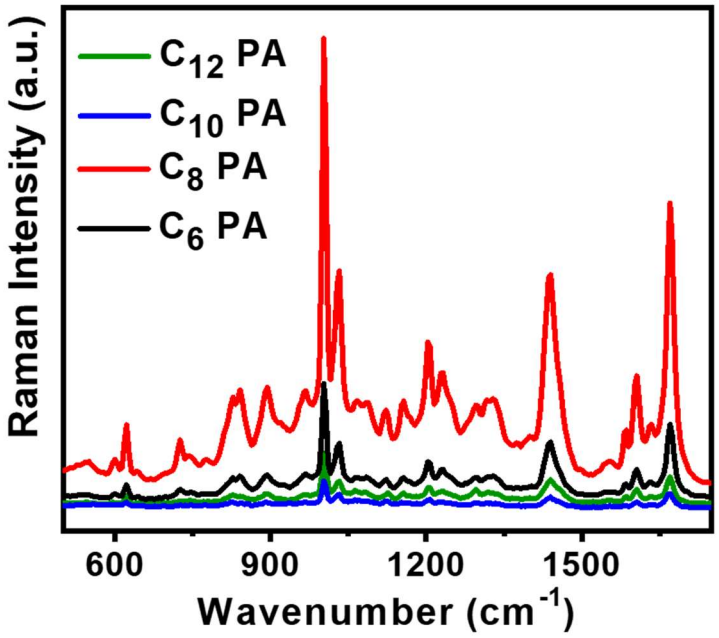

Figure S8: Raman spectra exhibiting peaks for the amino acids present in the peptide amphiphiles, **C_nPA**.

Surface elemental analysis from XPS

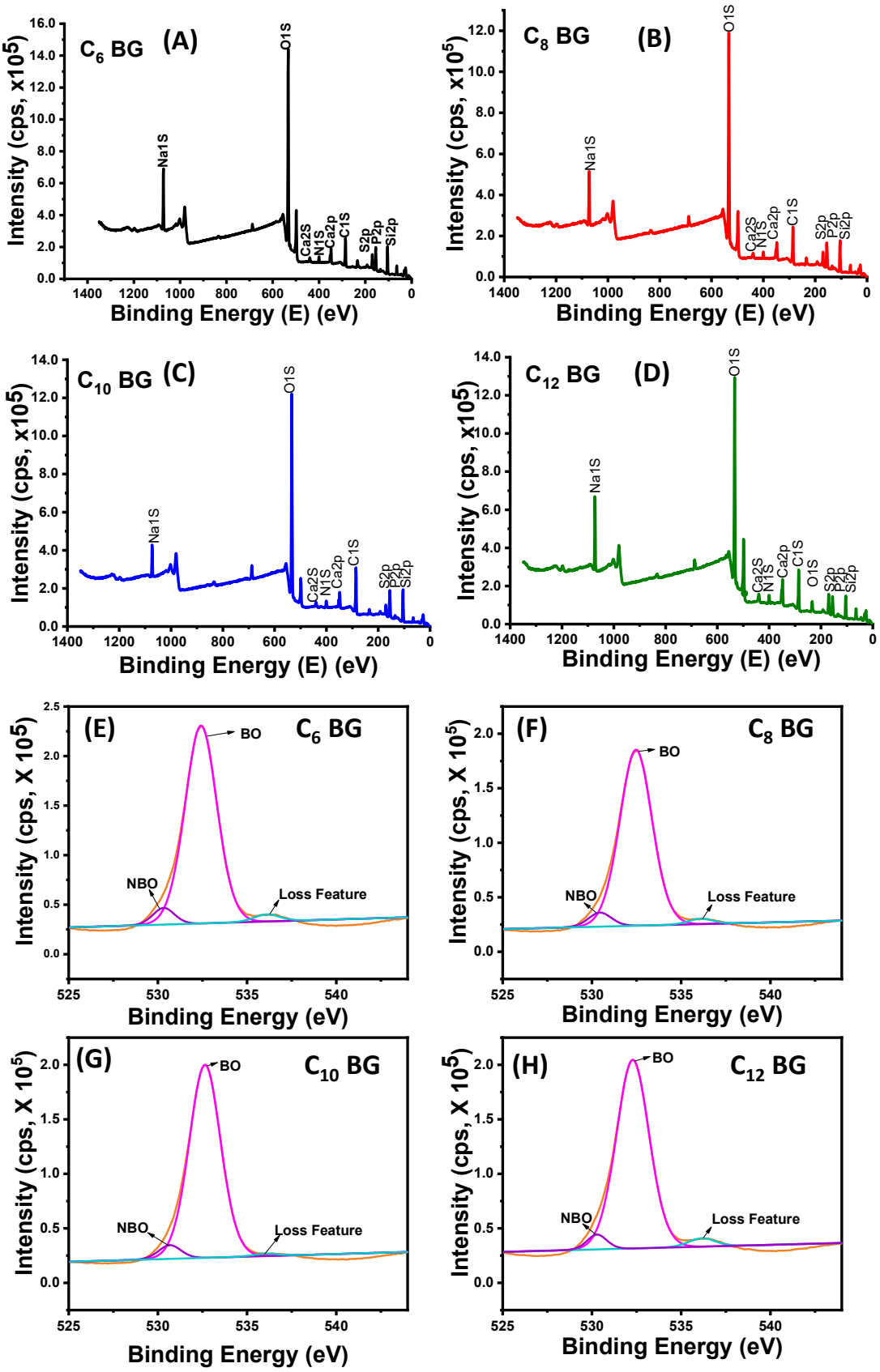

Figure S9: (A-D): XPS survey scan spectra showing well defined peaks for Na, Ca, Si, P, N, S, O, and C and **(E-H):** deconvoluted O1s Photoelectron spectra for **C_nBGs**.

Elemental Analysis from SEM-EDX

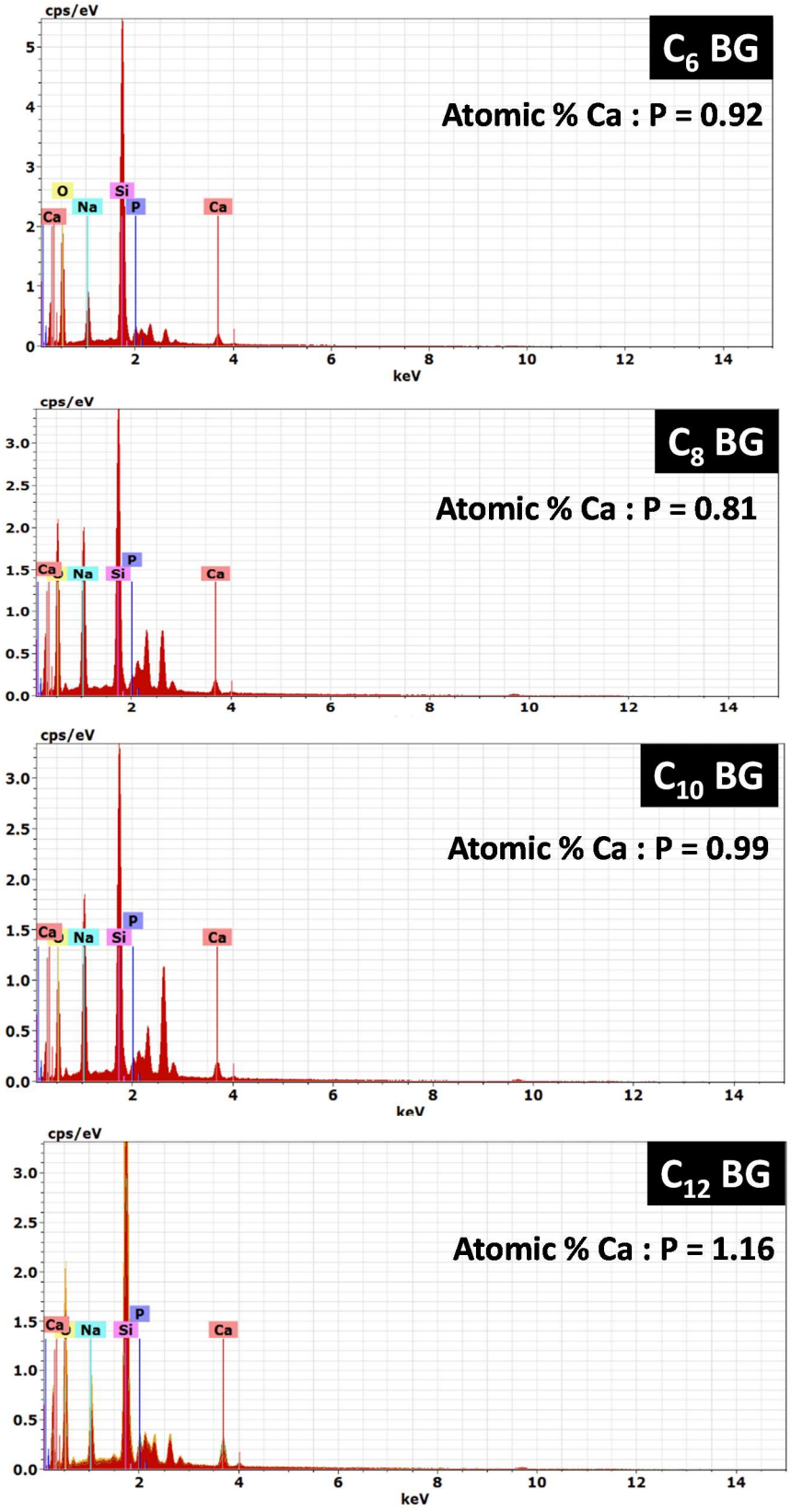

Figure S10: Atomic % Ca:P calculated from EDAX for bioglass composites, **C_nBG** before immersion in SBF. Ca:P ratio is calculated from average of three measurements.

Mechanical studies

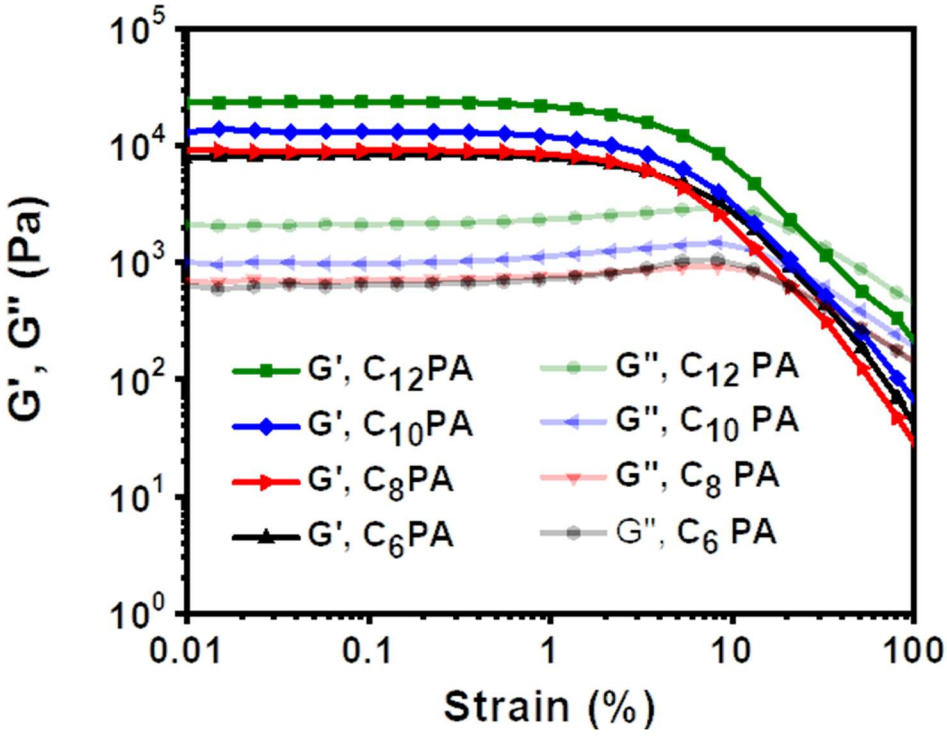

Figure S11: Amplitude sweep rheology for **C_nPA** with strain 0.01 to 100 % at constant angular frequency of 10 rad/s for 1 w/v% peptide hydrogels with 15 mM SPB as crosslinker at 25 °C.

Table S1: Critical strain and yield stress calculated from amplitude sweep rheology for **C_nBG**

Sample	Critical Strain	Yield Stress
C_6 BG	13.12 %	5720 ± 50 Pa
C_8 BG	7.37 %	7670 ± 150 Pa
C_{10} BG	5.29 %	5810 ± 80 Pa
C_{12} BG	3.11 %	3610 ± 180 Pa

Yield stress values represent mean ± SD calculated from triplicates experiments.

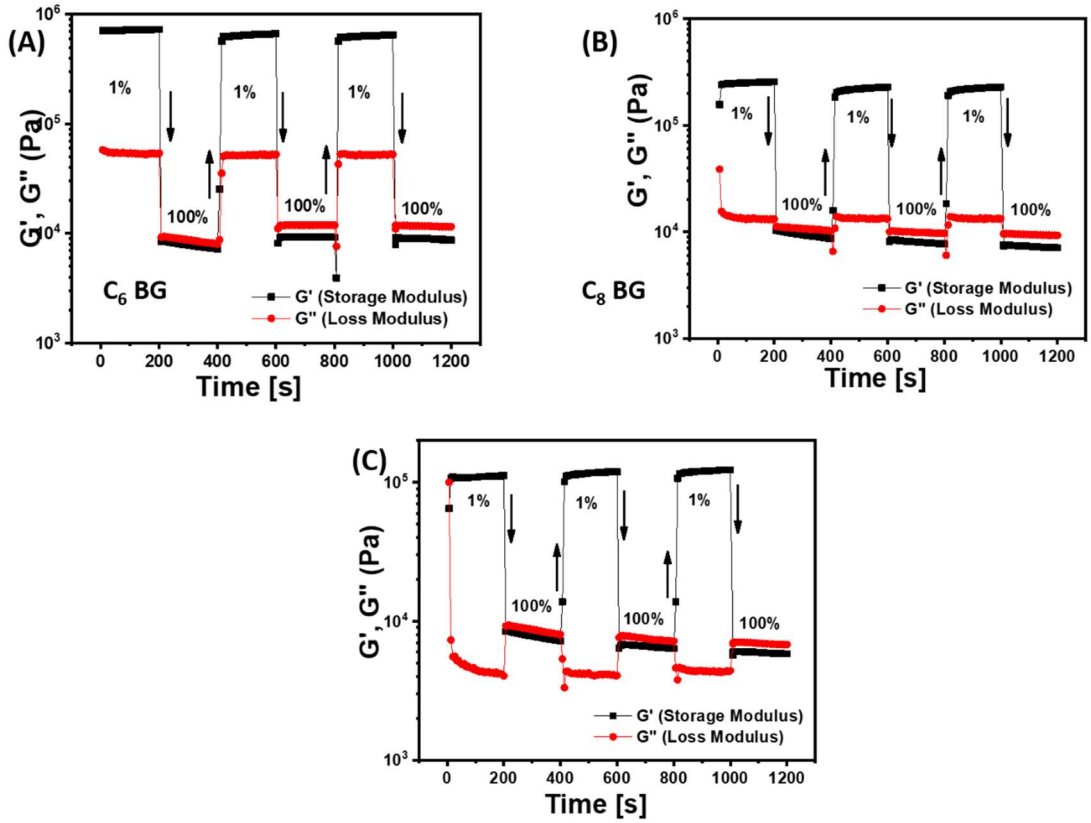

Figure S12: Thixotropic studies upon applying alternative cycle of high (100%) and low strains (1%) at a constant angular frequency of 10 rad/s for (A) **C_6BG,** (B) **C_{10}BG** and (C) **C_{12}BG**.

Self-healing and injectability studies

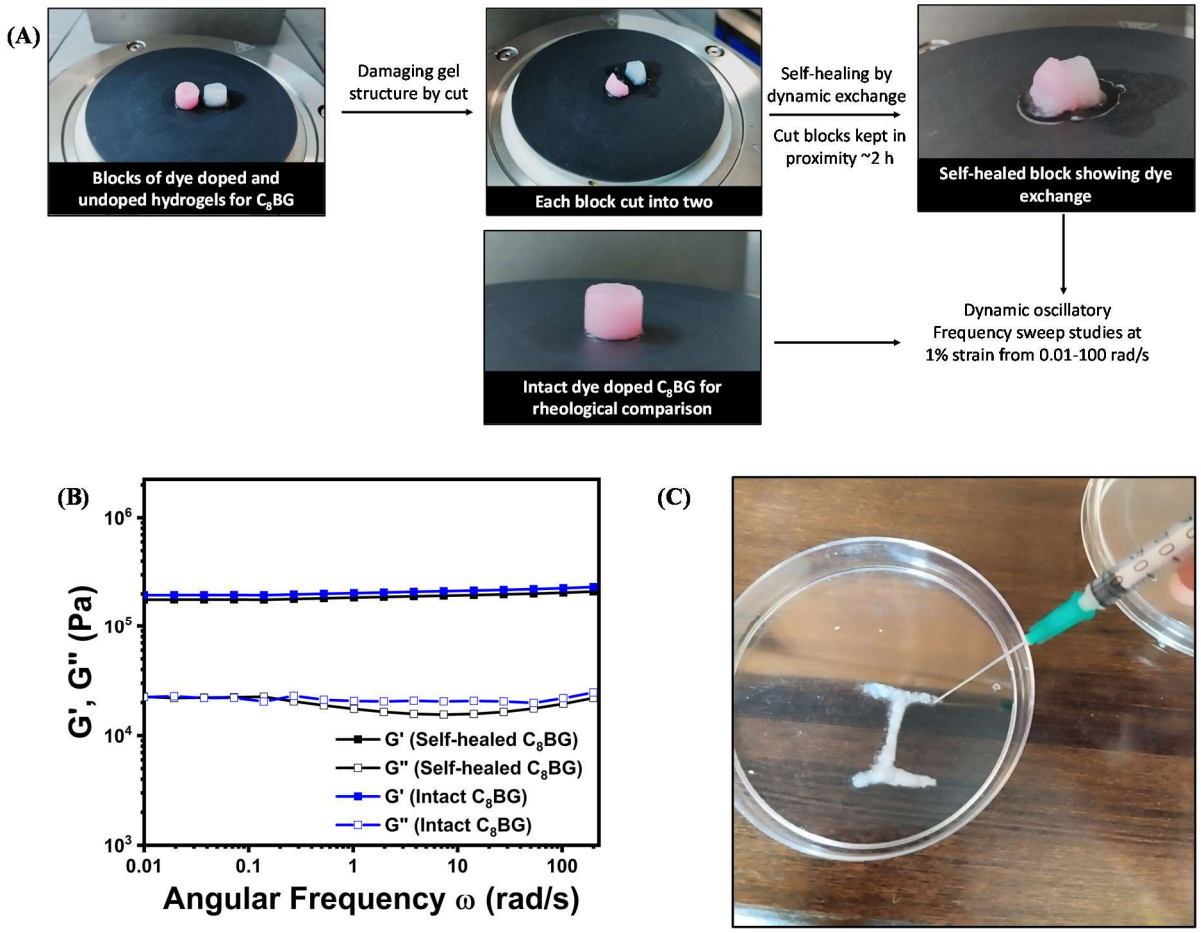

Figure S13: (A) Stepwise protocol for self-healing study for **C_8BG** composite. Self-healed gel refers to the mixed block (dye doped and undoped) hydrogel; Intact gel refers to the dye-doped uncut single block. (B) Comparative frequency sweep showing similar *G'* values to indicate recovery to the original strength of gel after self-healing. (C) Injectability of **C_8BG** composite on passing through syringe enabling desired extrusion pattern (alphabet **I** is shown here).

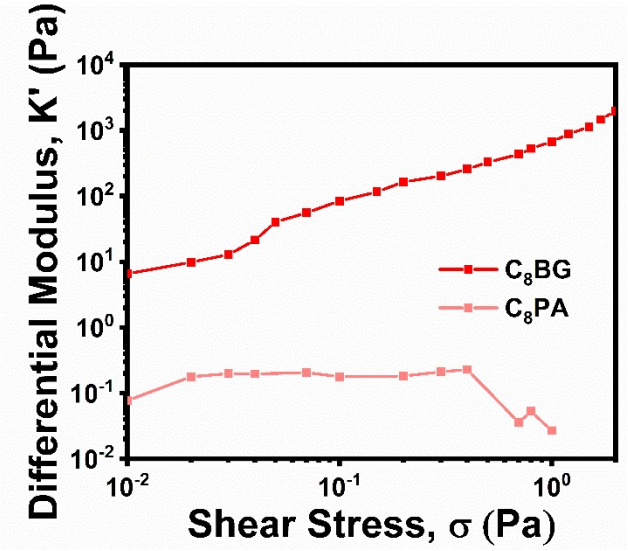

Figure S14: Plot of differential modulus *vs* shear stress of **C_8BG** depicting non-linear elasticity manifesting as strain-stiffening response that was absent in **C_8PA** accounting for lack of reinforcement contributions from bioglass.

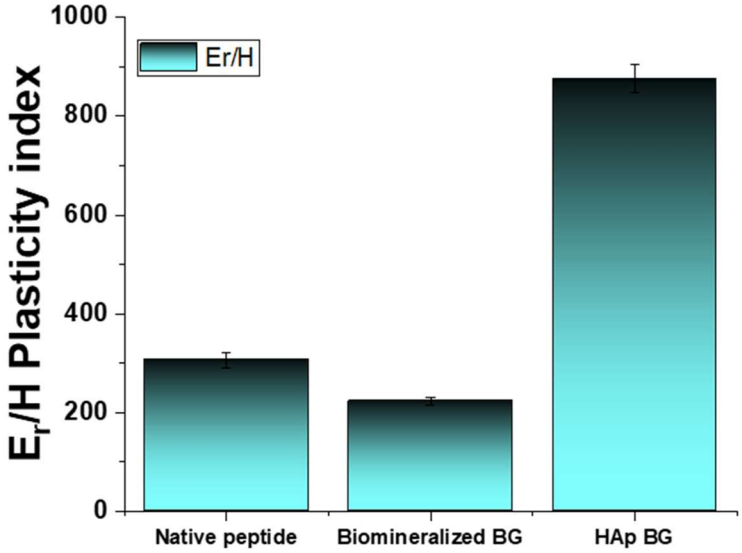

Figure S15: Plasticity indices of stages of templated bioactive glass derived from nanoindentation **C_8PA**, **C_8BG** and **C_8HAp** (**C_8BG** after 25 days SBF immersion). (Data represents mean ± SD, n = 2)

Elemental Mapping from TEM

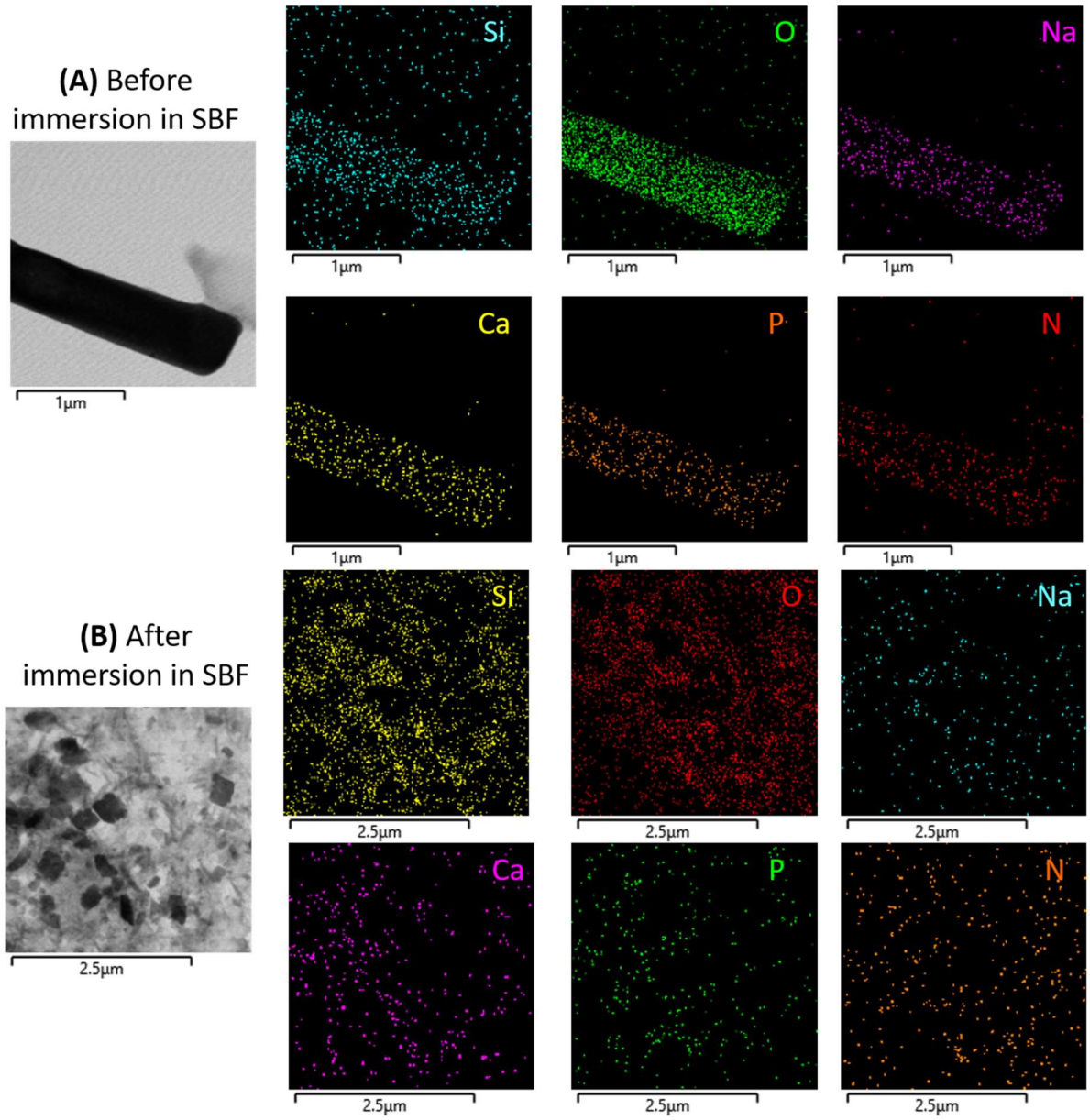

Figure S16: TEM elemental mapping for the distribution of bioglass ions namely Si, O, Na, Ca, P and N on the surface of **C_8BG** (A) before and (B) after immersion in simulated body fluid.

Hydroxyapatite deposition visualized through SEM

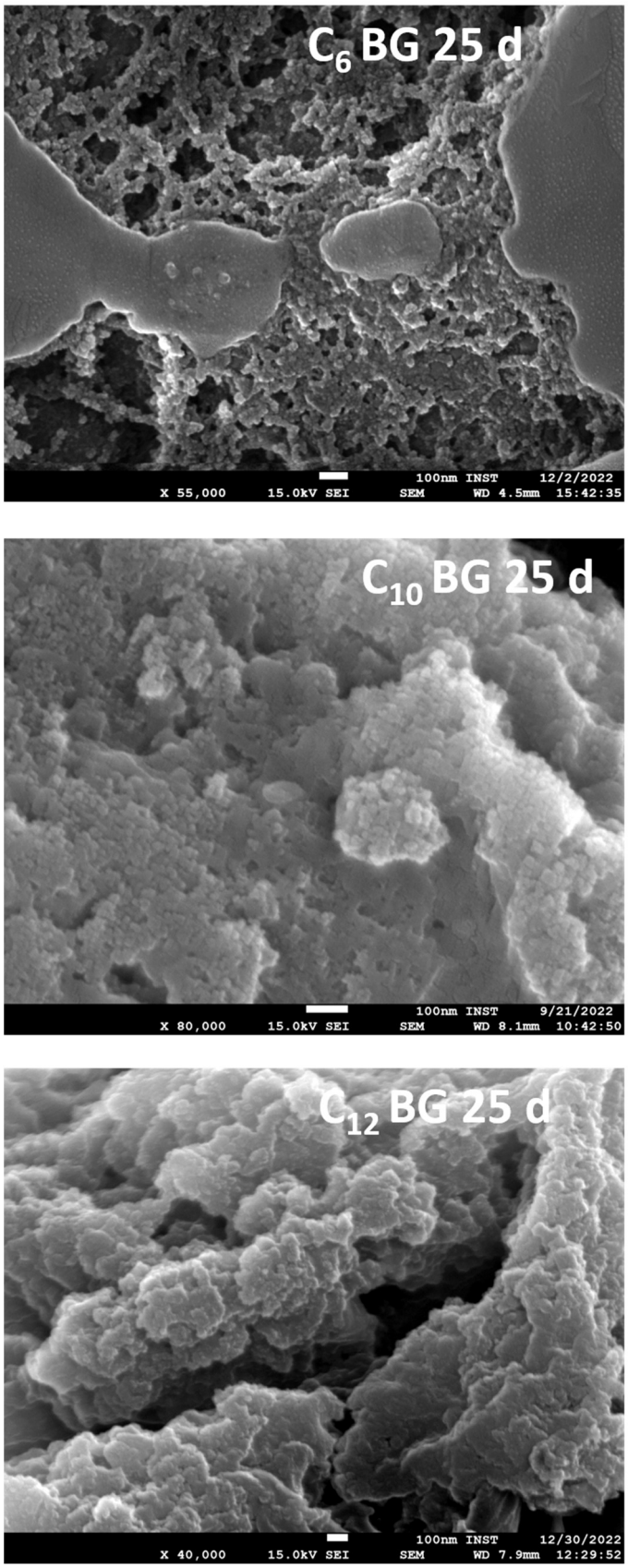

Figure S17: SEM images for surface altered layers of **C_6BG**, **C_{10}BG** and **C_{12}BG** upon immersion in SBF for 25 days showing deposited HAp (Scale bars = 100 nm).

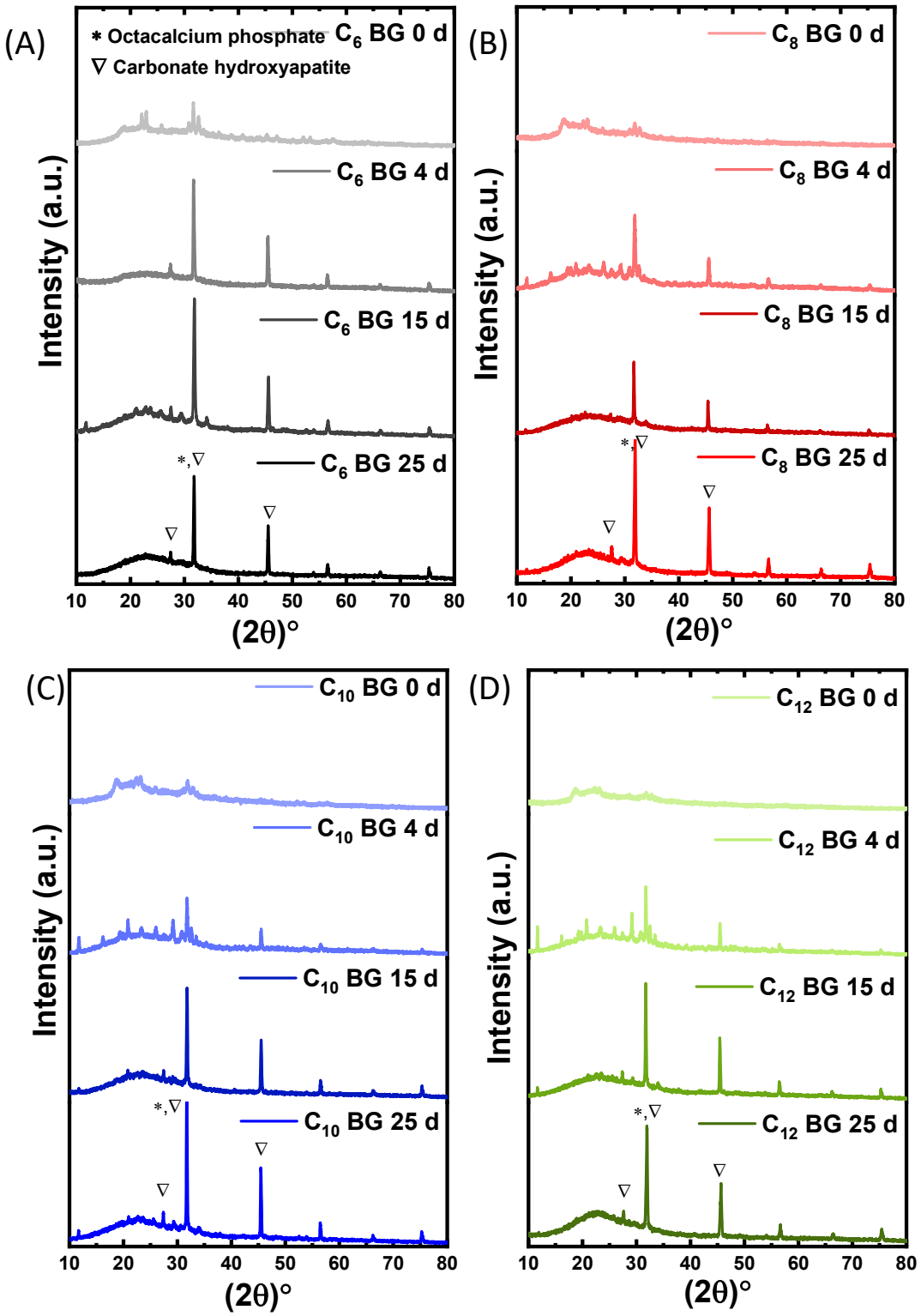

Figure S18: Time dependent evolution of biphasic calcium phosphate crystallinity monitored using XRD in (A) **C_6BG**, (B) **C_8BG,** (C) **C_{10}BG** and (D) **C_{12}BG**.

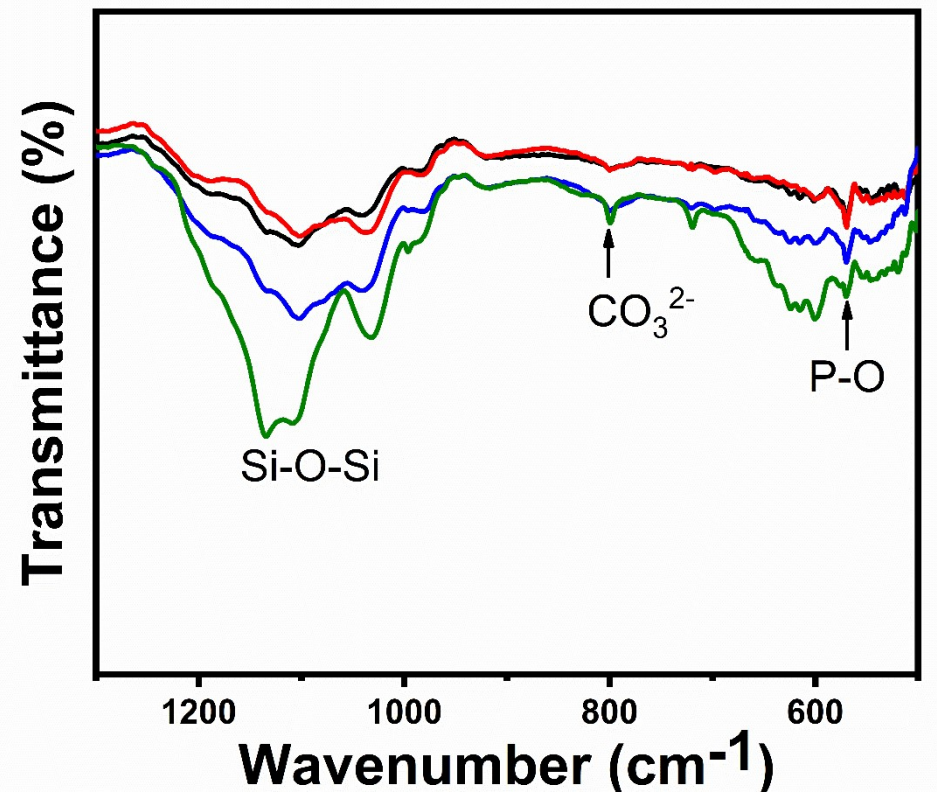

Figure S19: FTIR Spectra of **C_nBG** composites showing increase in vibrational bands for CO_3^{2-} and PO_4^{3-} after immersion in SBF for 25 days.

Quantitation for hydroxyapatite formation

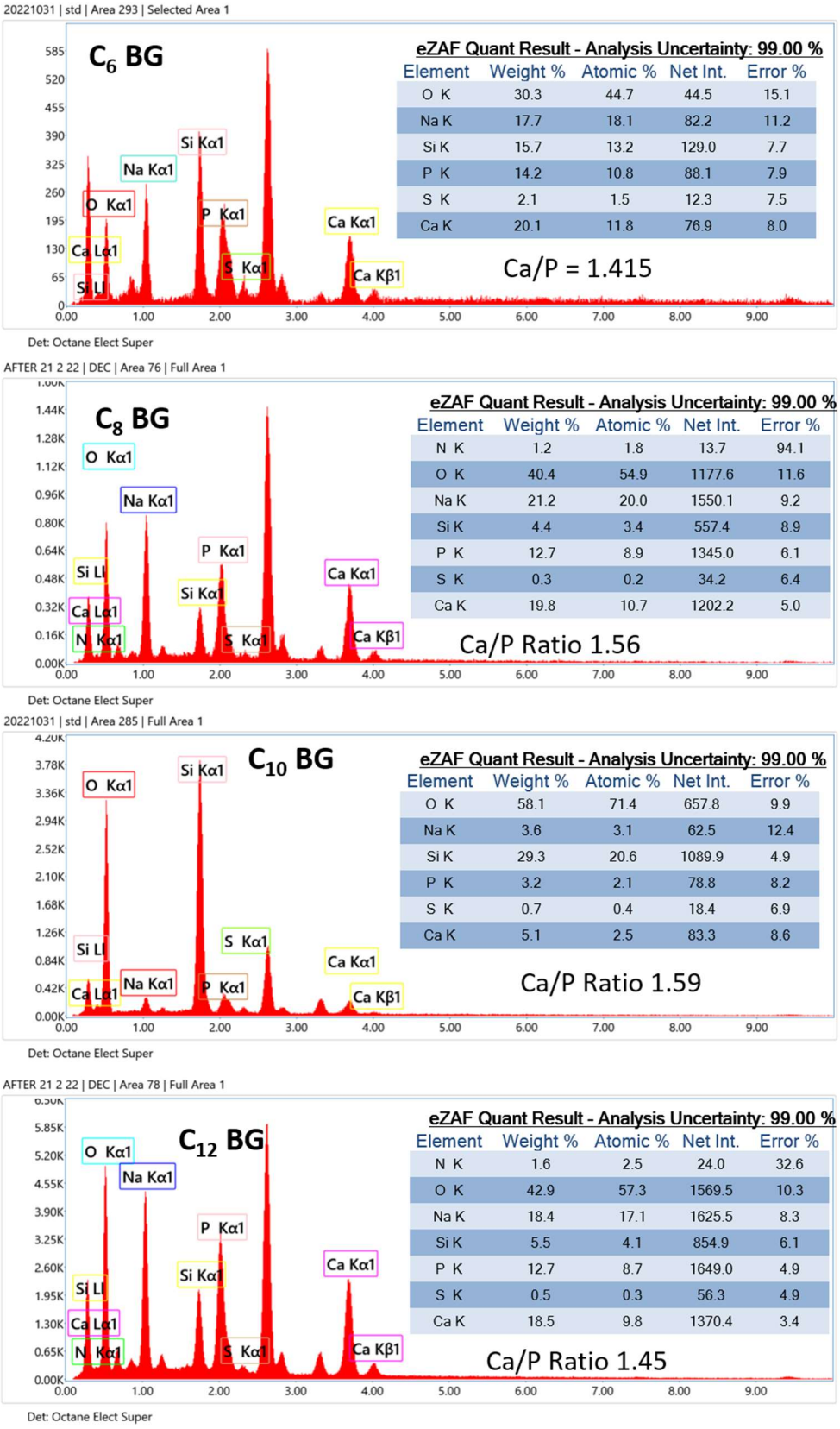

Figure S20: Weight % Ca:P ratio of **C_nBG** derived from EDX using SEM (after 25 days SBF immersion). All EDX measurement were recorded in triplicates and averaged to provide the % Ca:P ratio.

Cell adhesion

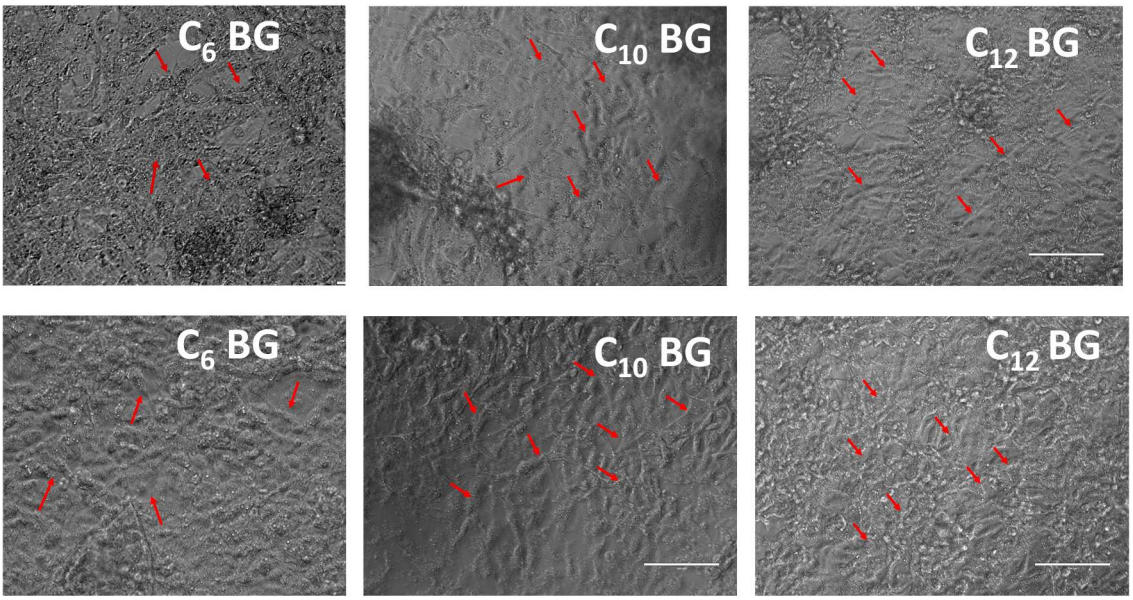

Figure S21: Evaluation of cellular morphology of U2OS cells through bright field microscopy on hydrogel surfaces of **C_6BG**, **C_{10}BG** and **C_{12}BG** for 24 (upper panel) and 48 hours (lower panel) respectively. Red arrows depict cells adhered on the matrix initiating spreading marked by the change in morphology. All scale bars = 100 nm.

Live/dead assay

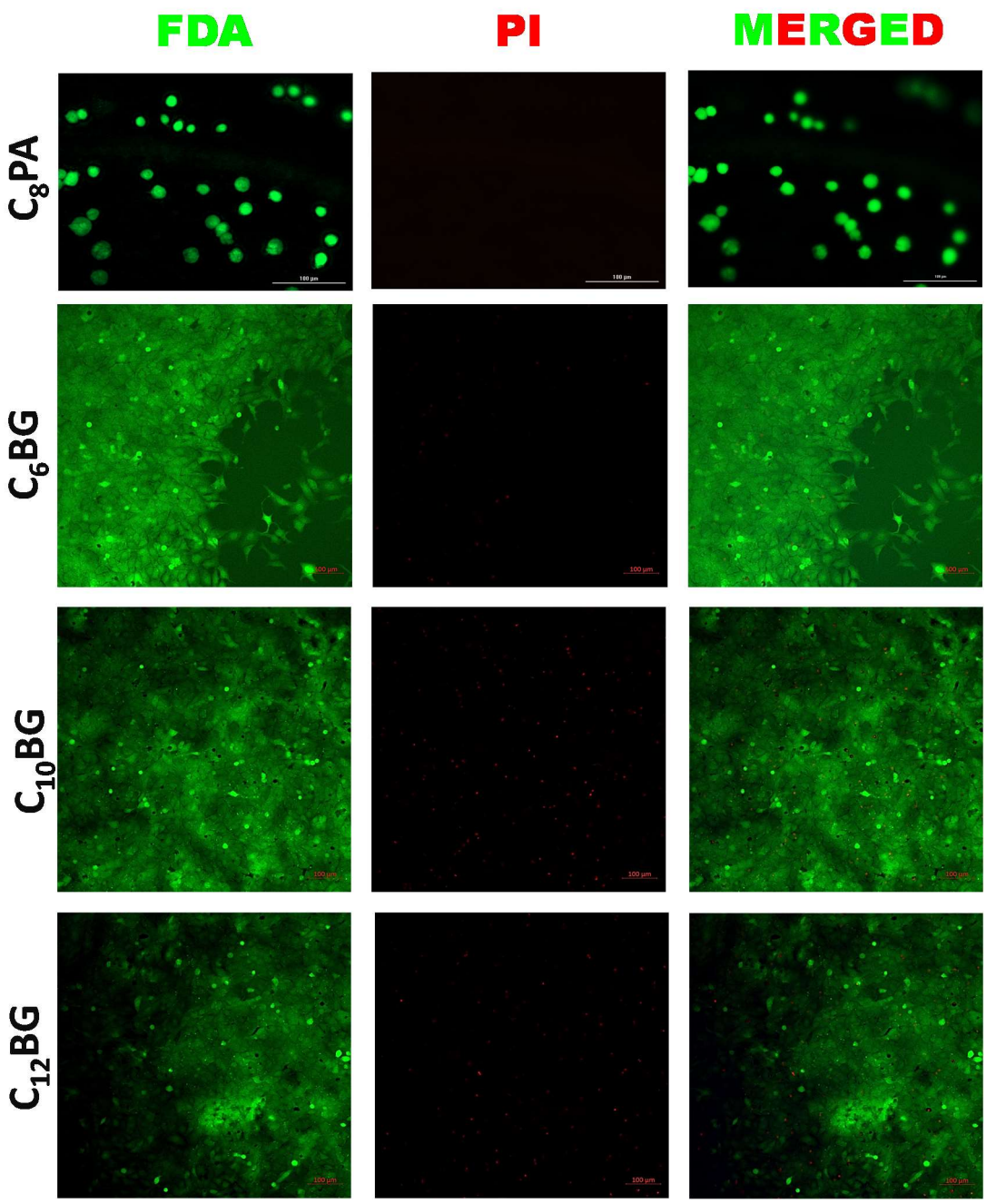

Figure S22: Confocal microscope images showing Live/dead cell assay as stained by FDA/PI for U2OS cells seeded on **C_nBG** matrices for 5 days with **C_8PA** as a control (Top panel).

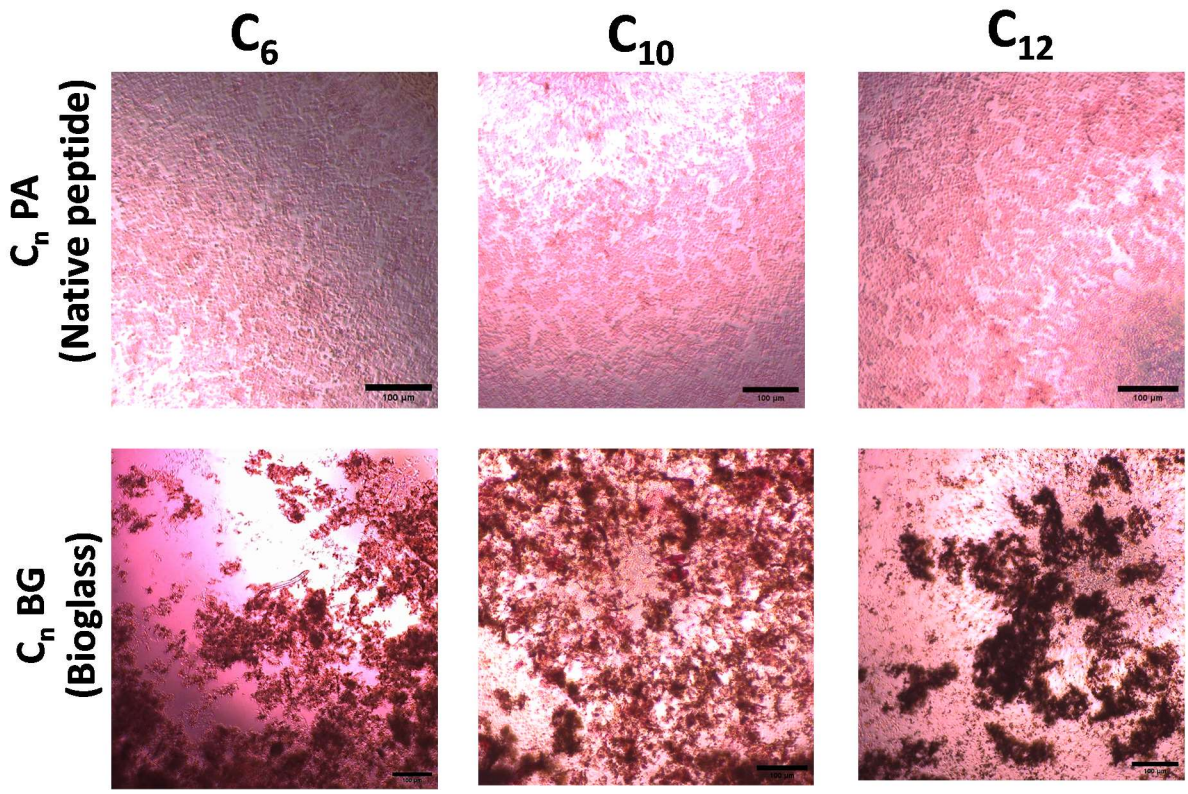

Figure S23: Alizarin Red-S staining to visualize the Ca deposits during cell proliferation and maturation of the osteoblast.